communications materials

Article

https://doi.org/10.1038/s43246-024-00623-z

Bio-responsive polymers for dual $^{31}P/^{19}F$-magnetic resonance to detect reactive oxygen species in vivo

Check for updates

Natalia Jirát-Ziółkowska[1,2], **Kateřina Sulková**[1,3], **Lucie Kracíková**[4,5], **Ladislav Androvič**[4], **Dominik Havlíček**[1,2], **Richard Laga**[4] & **Daniel Jirák**[1,2,6] ✉

Biocompatible metal-free agents are emerging as a promising alternative to commercial magnetic resonance (MR) contrast agents, but there is an additional need for novel probes with enhanced responsiveness in preclinical MR testing to effectively target diverse pathological conditions. To address this, we develop hydrophilic phospho-/fluoropolymers as dual MR probes. Incorporating thiophosphoester groups (P = S) into the polymer structure produces a distinct chemical shift (~59 ppm) in phosphorus MR (^{31}P-MR), reducing biological signals interference. Reactive oxygen species (ROS) oxidize the P = S groups, causing a detectable shift in ^{31}P-MR, enabling precise localization of ROS, abundant in inflammation and cancer. To enhance this capability, bioinert trifluoromethyl groups (CF_3) are added, creating a "hotspot" for fluorine MR (^{19}F-MR), aiding in vivo localization. Both in vitro and in vivo testing demonstrate the probe's high specificity and responsiveness, underscoring its potential as a sensitive ROS sensor and dual MR-traceable tool in cancer research.

Magnetic resonance imaging (MRI) is a widely adopted noninvasive diagnostic modality for visualizing internal body structures and monitoring physiological and pathophysiological conditions. Owing to the high hydrogen content in living organisms, particulary in water and organic molecules, proton magnetic resonance imaging (^{1}H-MRI) emerges as the predominant MRI technique in clinical applications. The nearly 100% natural abundance of the ^{1}H isotope and its advantageous intrinsic properties, such as a spin of ½ and a gyromagnetic ratio (γ) of 42.6 MHz T^{-1}, render it easily detectable at the relatively low magnetic fields employed in clinical scanners (1.5 T). Although ^{1}H-MR imaging is commonplace, the administration of contrast agents can enhance differentiation between healthy tissues and pathologies. However, clinically approved contrast agents containing gadolinium raise concerns due to potential toxicity, accumulation[1], and limited ability to provide additional information on tissue pathology. Consequently, there is a growing imperative to develop gadolinium-free contrast agents or probes to enhance the safety of MR imaging and the precision of pathology detection. ^{1}H-MRI provides valuable insights into the morphology and composition of tissues in the body. Nevertheless, to garner complementary information on tissue function, metabolism, and physiology beyond the capabilities of traditional proton MRI, specialized MR techniques utilizing isotopes other than hydrogen, X-nuclei MRI, are currently under development. Among the various nuclei applicable in X-nuclei MRI – such as ^{13}C, ^{17}O, ^{23}Na, ^{19}F, and ^{31}P – techniques for imaging phosphorus and fluorine have attracted considerable interest in recent years[2–14]. One of the promising X-nuclei, phosphorus, is characterized by the stable natural monoisotope ^{31}P possessing a nonzero magnetic moment with a spin value of ½ and a γ of 17.2 MHz T^{-1}. Notably, the magnetic sensitivity of ^{31}P is 60% lower than that of ^{1}H. Despite phosphorus being roughly 10 times less abundant in the human body mass and having ~2.5 times less magnetic momentum than hydrogen protons, sensitive radiofrequency coils enable the detection of phosphorus even at the low magnetic fields typically used in clinical settings. Historically, ^{31}P-MR has primarily been used to assess cell membrane composition, phosphorylated metabolite levels, the bioenergetic status of organs and tissues, and intracellular pH levels[15–22]. In recent years, its broader potential has been explored using responsive phosphorus and iron-based probes[4,5], but its tendency to significantly overlap with physiological background signals within the MR frequency range remains a challenge. The solution to these problems could

---

[1]Institute for Clinical and Experimental Medicine, Prague, Czech Republic. [2]Institute of Biophysics and Informatics, First Faculty of Medicine, Charles University, Prague, Czech Republic. [3]Division of Systems Biology of Signal Transduction, German Cancer Research Center (DKFZ), Im Neuenheimer Feld 280, Heidelberg, Germany. [4]Institute of Macromolecular Chemistry, Czech Academy of Sciences, Heyrovského nám. 2, Prague, Czech Republic. [5]Faculty of Chemical Technology, University of Chemistry and Technology, Prague, Czech Republic. [6]Faculty of Health Studies, Technical University of Liberec, Liberec, Czech Republic. ✉e-mail: daji@ikem.cz

be a probe with a different chemical shift in phosphorus MR, as proposed in our previous publication[6], where the in vivo use requiring specific exogenous probes for accurate measurement was discussed.

Another X-nucleus frequently investigated for clinical MRI applications is fluorine-19 (^{19}F-MRI). This monoisotope possesses not only a negligible physiological concentration but also a high gyromagnetic ratio (40.1 MHz T^{-1}), with MR specificity and sensitivity comparable to hydrogen (83% of ^{1}H)[23]. Therefore, overlaying the ^{19}F-MR signal from exogenous probes onto the anatomical background obtained by ^{1}H-MRI measurements facilitates monitoring the biodistribution and pharmacokinetics of probes within the body. The fluorine-based probes are widely examined in the preclinical studies[2,3,7–13] and first trials of clinically usable probes were published[14]. Importantly, ^{19}F-MR can be performed using common scanners and radiofrequency coils, requiring only minor hardware adjustments. However, compounds containing fluorine are often hydrophobic and poorly soluble in water, limiting their clinical utility to a significant extent.

Previous X-nuclei research, including work from our group and others[2–14,24,25], has demonstrated that hydrophilic biocompatible phospho- and fluoro-based MR probes serve as suitable probes for MR imaging and spectroscopy (MRS). In comparison to low molecular weight probes, these macromolecular compounds exhibit enhanced solubility, a higher P/F atoms content, and prolonged biological half-life. Moreover, their structures, compositions and dimensional characteristics can be specifically tuned, allowing for elimination from the organism after measurements. They are also easily modifiable for use as drug carriers[26,27]. Due to their greater hydrodynamic size, they can passively accumulate in specific pathologies, such as tumors through the enhanced permeability and retention (EPR) effect[28] or inflammation via extravasation through leaky vasculature and subsequent inflammatory cell-mediated sequestration[29]. This accumulation can be exploited for targeted imaging of these pathologies.

Fluoropolymers offer the advantage of being bioinert and easily distinguishable, providing a ^{19}F-MR signal without the biological background. However, they are not without limitations. Frequently hydrophobic, their solubility tends to decrease with increasing fluorine content. In contrast, certain phoshpopolymers can be design to be highly soluble in aqueous solutions, even with a high phosphorus content, and are biocompatible, and, in some cases, biodegradable. Nonetheless, commonly used phosphopolymers like as poly(2-methacryloyloxyethyl phosphorylcholine) (pMPC), poly(phosphoesters), or some poly(phosphazenes) often exhibit a chemical shift similar to naturally occurring biomolecules, making their ^{31}P-MR signal challenging to distinguish from the signal of surrounding tissues[30,31]. Signal recognition of certain phosphopolymers can be enhanced, as demonstrated in our prior research[6], where we utilized a unique phosphopolymer in which one of the oxygen atoms in the phosphoester groups ($P = O$) was replaced with sulfur to form a thiophosphoester groups ($P = S$)—changing the chemical shift in phosphorus MR.

While various fluoropolymers or phosphopolymers for in vivo MR use have been described in recent literature, a significant scientific challenge remains in the development of probes capable of detecting changes in pathophysiological processes associated with the onset of specific disorders. One indicator of physiological abnormalities is the tissue-specific level of reactive oxygen species (ROS). ROS encompass a group of naturally occurring, chemically reactive compounds containing oxygen, including the superoxide anion radical, hydroxyl radical, hydroperoxyl radical, singlet oxygen, and various nitrogen and hypochlorite radicals, all more reactive than ground-state oxygen[32]. Typically generated through the partial reduction of molecular oxygen via both endogenous (physiological) and exogenous (environmental) oxidative processes within biological systems[33], ROS are produced in many cellular compartments, with mitochondria being a major source. At moderate levels, ROS are required for several cellular functions, including gene expression[34], and are involved in diverse biological processes such as host defense, signaling, tissue development, injury response, as well as hypertension and tumor development[35–38]. Inflammation sites and tumors are generally characterized by a significant increase in ROS concentration[39], commonly formed by both the immune system and cancer cells to create a microenvironment unique among healthy tissues. Importantly, changes in ROS levels are also associated with chemotherapy and radiotherapy[39–41].

The standard methods for ROS-detection in vitro are based on the fluorescence, which is highly sensitive, but not clinically relevant. In diagnostics there are several advanced techniques for detecting ROS, such as positron emission tomography (PET), ultraweak photon emission imaging (UPE), and optical and photoacoustic imaging, have been integrated into experimental medical applications[40–46]. However, these methods face limitations that hinder their application in clinical practice. PET exposes the patients to ionizing radiation, UPE is restricted to superficial areas, and optical imaging encounters challenges with poor tissue penetration[47]. Encouragingly, X-nuclei MRI holds promise in this realm, but its use is contingent upon the development of suitable probes. As cancer-specific factors are generally lacking in CAs MRI methodology, no ROS-detecting method is currently available in MR. To address those limitations, we designed a water-soluble polymer probe with high phosphorus and fluorine content and specific responsivity. Hypoxia, measured using MR methods, is tightly connected with oxidative stress and ROS-targeting therapies used in radiotherapy usually encounter the problem of ROS generation overwhelming the antioxidant mechanisms of the cell, leading to oxidative stress. Thus, ROS can play both pro- and anti-tumor role in a context-dependent manner and its sensitive detection would be highly beneficial.

The primary aim of this investigation is to introduce an innovative method utilizing dual ^{31}P/^{19}F-MR for in vivo localization and assessment of tumor tissue employing hydrophilic phospho-/fluoropolymer responsive to ROS changes. Initially, ROS production was evaluated in vitro using a highly sensitive fluorogenic reagent to detect extracellularly released oxidation products. Subsequently, we monitored their impact on the chemical shift of the polymer probe under various oxidative conditions using ^{31}P-MRS across various cell lines, validating its performance in vivo using an murine tumor model. Despite the ability of modern methods to detect ROS changes, quantifying alterations in their concentrations remains a challenge.

A crucial aspect of our analysis involved assessing the performance of our biocompatible, ROS-responsive polymer probe under conditions closely resembling clinical magnetic field strengths, specifically 4.7 T. Demonstrating high specificity and responsiveness, the probe showed its capacity to detect pathophysiological conditions characterized by the presence of ROS. While ^{31}P-MRS was used to detect ROS produced in a tumor environment, fluorine MR spectroscopy and imaging were employed to monitor changes in the biodistribution of the probe over time. As an in situ reference, fluorine adeptly localized the probe precisely in instances where the phosphorus signal disappeared due to shifting caused by ROS-induced oxidation. We anticipate that the dual MR probe presented in this study will offer new insights into the detection, diagnosis and subsequent treatment of tumors and inflammatory diseases.

Results

Synthesis of the polymer probes

To track in vivo biodistribution of the exogenously administered probe simultaneously with tissue-specific ROS production using ^{31}P/^{19}F-MR, the structure of the probe was modified to provide a sufficiently high and sustained signal-to-noise ratio (SNR) that would be easily distinguishable from the signals generated by the naturally occurring biomolecules. The probe also needed to be sufficiently responsive and sensitive to change its chemical composition in the presence of ROS. For these purposes, we developed custom biocompatible polymer probes containing thiophosphoester (referred to as $P = S$ for simplicity) and/or trifluoromethyl (CF_3) groups. While the $P = S$ groups served as an ROS scavenger detectable by ^{31}P-MR, the CF_3 groups enabled the probe to be precisely localized using ^{19}F-MR. Specifically, the reversible addition–fragmentation chain transfer (RAFT) polymerization technique in the presence of dithiobenzoate-based chain transfer agent and azoinitiator was used to produce a water-soluble O-(2-(methacryloyloxy)ethyl) O-(2-(trimethylamoniumyl)ethyl)

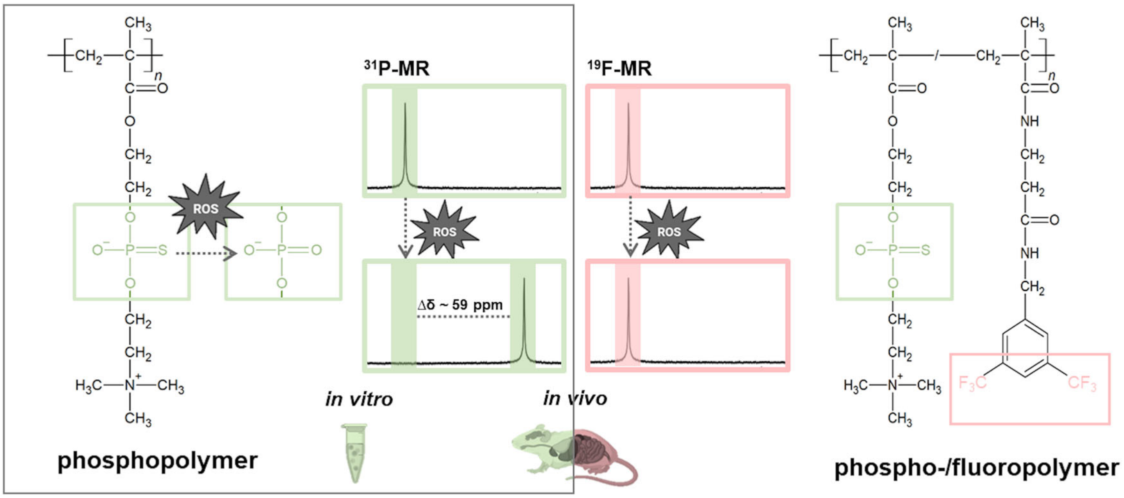

Scheme 1 | Visual representation of the in vitro and in vivo application of the polymers.

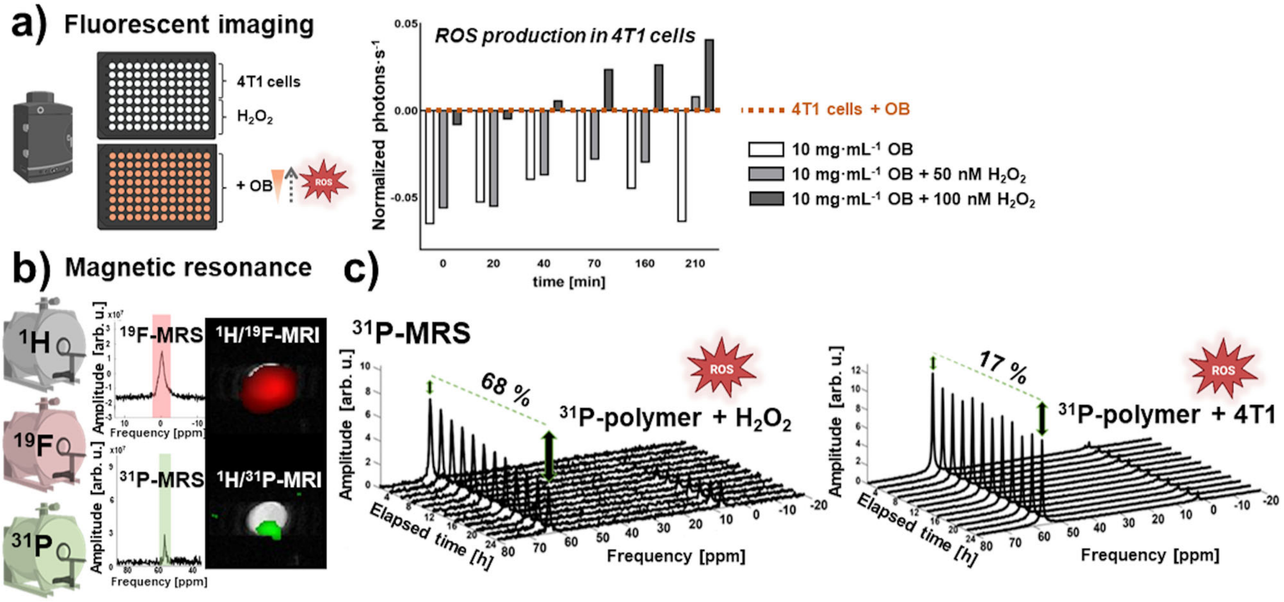

Fig. 1 | Results of in vitro experiments. a Fluorescence measurement of ROS production in 4T1 cells using the nonfluorescent dye OxyBURST Green H_2HFF BSA (OB), which is oxidized by ROS to the fluorescently active derivative. Results are presented as the total emission (photons·s^{-1}) in controls, normalized to the signal of 4T1 cells in a medium with 10 mg·mL^{-1} OB over time. **b** ^{31}P/^{19}F -polymer in phantom (c^P = 100 mM; V = 100 μL) measured using ^{19}F- and ^{31}P-MRS and ^{1}H/^{19}F/^{31}P-MRI. ^{19}F- (red) and ^{31}P-(green) MRI data are overlaid with ^{1}H-MRI signal. **c** Relative ^{31}P-MRS amplitude decreases (%) in different ROS-triggered oxidative conditions: ^{31}P-polymer with (left) H_2O_2 and (right) 4T1 cells, reflecting the oxidation of the P = S (Δδ ~ 60 ppm) signal to the P = O (Δδ ~ 0 ppm) signal over time.

phosphorothioate (TMPC)-based homopolymer of zwitterionic character (^{31}P-polymer) and a statistical copolymer of TMPC with a methacrylamide comonomer bearing the bis(trifluoromethyl)benzylamine group (Ma-βAla-BTFBA), referred to as the ^{31}P/^{19}F-polymer (for structures, see Scheme 1; the reaction scheme is presented in Supplementary Fig. 1). While the ^{31}P-polymer was prepared by direct polymerization of the TMPC monomer, the ^{31}P/^{19}F-polymer copolymer was obtained by a post-polymerization aminolytic reaction of the TT-activated precursor p(TMPC-*co*-Ma-βAla-TT) with BTFBA. The molecular weights were 22.1 kg·mol^{-1} for the ^{31}P-polymer and 16.7 kg·mol^{-1} for the ^{31}P/^{19}F-polymer. Both (co)polymers were characterized by low dispersity ($Đ \leq 1.1$).

Chemical structures of the phosphopolymer (^{31}P-polymer) and phospho-/fluoropolymer (^{31}P/^{19}F-polymer) with assigned experimental use in the study.

ROS production under hypoxic conditions

ROS production was confirmed by fluorescence measurements of murine mammary carcinoma 4T1 cell line, derived from mouse breast cancer, where the conversion of OxyBURST Green H_2HFF BSA (OB) dye to its fluorescent derivative was observed. Notably, the 4T1 cell line exhibited a higher total fluorescence emission ratio compared to the medium with OB alone and OB with different concentrations of hydrogen peroxide H_2O_2 (up to 210 min for 50 nM and up to 40 min for 100 nM) (Fig. 1). In the control samples, the highest signal increase over time was observed in the OB samples treated with 100 nM H_2O_2. The mentioned OB relevance using extracellular, rather than intracellular ROS production, was confirmed through complementary experiments. Specifically, the internalization process in PANC-1 (evaluated via confocal microscopy; Dy647 dye) and RAW264.7 macrophages (assessed using ^{19}F-MRS on 14 T MR) demonstrated decreased efficacy when employing the dual ^{31}P/^{19}F-polymer as

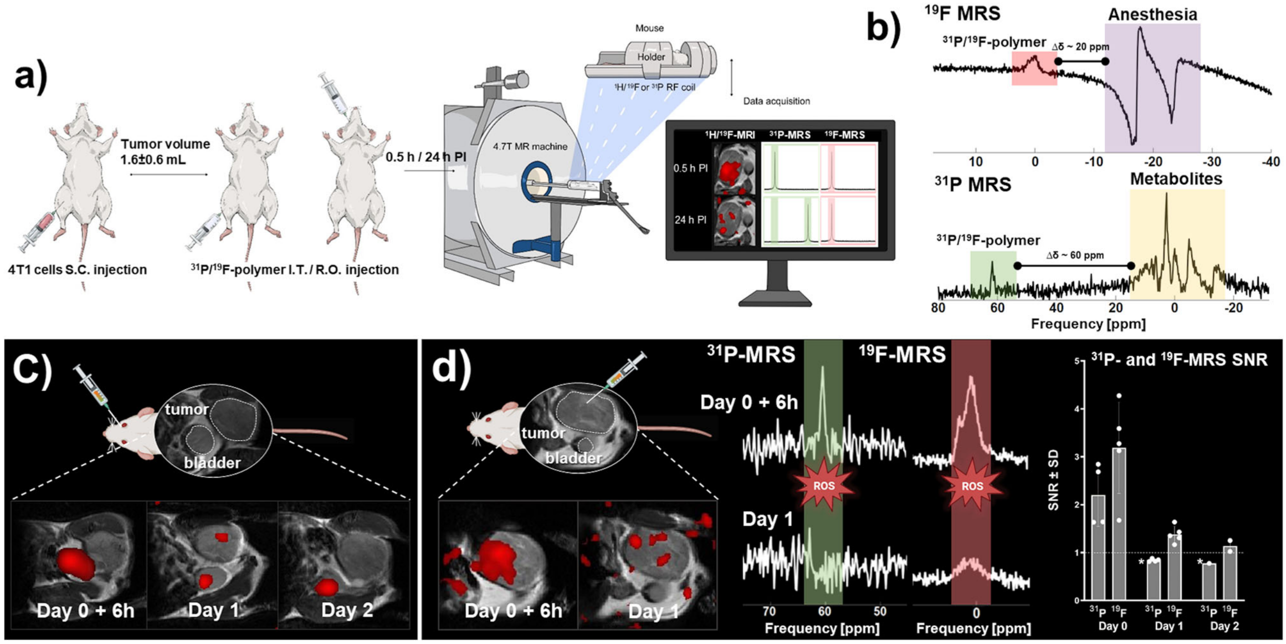

Fig. 2 | Results of in vivo experiments. a Experimental schematic outlining the steps including tumor induction, injection of ^{31}P/^{19}F-polymer, and MR measurement setup. **b** MR chemical shift between the ^{31}P/^{19}F-polymer and anesthesia (isoflurane; $\Delta\delta \sim 20$ ppm, ^{19}F-MRS), and between physiological signal (metabolites; $\Delta\delta \sim 60$ ppm, ^{31}P-MRS). **c** Results of proof-of-principle in vivo ^{19}F-MRI after retro-orbital ^{31}P/^{19}F-polymer injection. Overlaid ^{1}H/^{19}F-MRI with the fluorine signal highlighted in red. Results are visible 6 h (Day 0 + 6 h), 24 h (Day 1), and 48 h (Day 2) post-injection. **d** Results of in vivo ^{31}P-MRS and ^{19}F-MRS/MRI in response to ROS-triggered changes after I.T. ^{31}P/^{19}F-polymer injection. Overlaid ^{1}H/^{19}F-MRI and ^{19}F-MRS with fluorine signal presented in red, and ^{31}P-MRS data with the phosphorus signal highlighted in green; both measured 6- and 24-h post-injection (Day 0 + 6 h and Day 1). On the right, average SNR values of the ^{31}P/^{19}F-polymer injected I.T. for both ^{19}F- and ^{31}P-MRS; * indicates ^{31}P-MRS SNR values below the detection limit (<1); both measured 0.5–48 h post-injection (Day 0 to Day 2).

opposed to utilizing the ^{31}P-polymer alone and no fluorine signal from cells treated with the polymer overnight. The results are presented in Supplementary Fig. 2.

^{31}P-polymer MR signal changes under hypoxic conditions

The ^{31}P-MRS signal originating from the P = S groups within the phosphorus-based ^{31}P-polymer structure remained detectable across all tested conditions, including the short-time measurements. However, the reduction in signal amplitude varied among experiments (Fig. 1 and Supplementary Fig. 3). Consistent with previously ^{31}P-NMR findings, the first two highly oxidizing model conditions, involving aqueous solutions of H_2O_2 and sodium hypochlorite NaClO, similarly triggered a reduction in the signal[6]. In the presence of H_2O_2, the polymer underwent oxidation, leading to a 47% conversion of the signal from the P = S groups ($\Delta\delta \sim 60$ ppm) to the P = O groups ($\Delta\delta \sim 0.0$ ppm) within the first hour. Maximum oxidation of 68 % was reached after 24 h. Incubation of the probe in NaClO solution resulted in rapid and significant oxidation, evidenced by a remarkable 97% decrease in the P = S signal within one hour. Additionally, variations in ROS-triggered oxidation were noted among cell cultures: human leukemia monocytic THP-1 cells exhibited amplitude decreases of 14% (within the first 12 h) and 20% (at 24 h from onset), human prostate adenocarcinoma PC3 cells showed reductions of 13% and 19%, and 4T1 cells influenced P = S signal by 8% and 17%, respectively. No significant changes in signal shift or amplitude (0.33 ± 1.85%) were observed in the ^{31}P-MR spectra obtained from the polymer in the medium, even over an extended data collection period of 18 h. The viability of a series of PC3 cells stored in Eppendorf tubes at room temperature, similar to the conditions used for MR measurements, remained within a range of 90–93% at all time points (1–3 h) (data not shown).

The ^{31}P/^{19}F-polymer was measured using ^{31}P- and ^{19}F-MR spectroscopy and magnetic resonance spectroscopic imaging (MRS/MRSI) to determine signal sensitivity (Supplementary Fig. 4) and changes in the ROS-triggered signals. MRS data indicated frequency shifts in the signals suitable for further in vivo experiments, with high signal sensitivity achieved even over short measurement periods (scan time ST = 3 min). MRSI generated signals for both phosphorus (ST = 10 min) and fluorine (ST = 3 min). Under oxidative conditions, the phosphorus P = S signal decreased in accordance with the behavior of the ^{31}P-polymer. In contrast, the fluorine signal remained stable, confirming the stability of the polymer (Supplementary Fig. 5).

These results were successfully repeated on the clinical 3 T and preclinical 7 T MR scanner, where the ^{31}P-polymer with H_2O_2 underwent full oxidation after 24-h incubation (Supplementary Figs. 6, 7a, c).

In vivo MR of polymer biodistribution and oxidation-triggered signal changes

The high phosphorus content in the polymer provided a substantial MR signal, as evidenced by the high chemical shift of the P = S groups in ^{31}P-MR ($\Delta\delta \sim 60$ ppm) at low, nontoxic concentrations (Fig. 2a). This characteristic made the MR signal easily distinguishable from the biological background signals in vivo (~0 ppm). The quantified phosphorus MR signal originating from the P = S groups of the ^{31}P/^{19}F-polymer exhibited the same chemical shift as the previously tested ^{31}P-polymer containing TMPC monomer units only. Additionally, the fluorine signal displayed a shift in ^{19}F-MRS ($\Delta\delta \sim 20$ ppm) compared to the anesthesia signal (Fig. 2b), resulting in a 100% specificity. This shift serves as a crucial factor in enhancing the precision and accuracy of our in vivo imaging technique, as it guarantees a clear differentiation between the fluorine signal from the polymer and the background signal originating from the anesthesia.

Initial in vivo measurements of polymer biodistribution revealed significant accumulation of the polymer in the bladder, tumor (following intravenous I.V. injections via the lateral tail vein or retro-orbitally via the venous sinus R.O.), and kidneys (following I.V. injection via the lateral tail). The intravenous injection resulted in the highest ^{19}F-MR signal two days after polymer administration (Supplementary Fig. 7). No immediate signal was observed after the injection, with only a weak fluorine MRS signal detected on day one. Conversely, retro-orbital administration initially resulted in visible ^{19}F-MR signal solely in the bladder, with accumulation in tumor tissue observed one day after administration. The rest of the polymer was excreted in urine, evident from a strong signal in the bladder at all measurement points. No signal from the tumor was detected on the second day post-administration (Fig. 2c).

In subsequent in vivo analysis, mice underwent ^{31}P-MRS and ^{19}F-MRS/MRI at three-time points: immediately after the ^{31}P/^{19}F-polymer intratumoral (I.T.) injection, and then 24 and 48 h after administration (Fig. 2d). The ^{31}P-MRS signal of the polymer was detected immediately after injection in four out of five animals (SNR = 2.20 ± 0.65). On day one (24 h PI), a decrease in the phosphorus MRS signal was observed, indicating the conversion of the phosphorus signal from P = S to P = O due to ROS production in hypoxic cancer tissue. The SNR of the integral at this point (0.84 ± 0.03) was considered noise. Conversely, the ^{19}F-MRS signal was detected immediately after injection in all measured animals (SNR = 3.19 ± 0.95) persisting at 24 h (SNR = 1.38 ± 0.17) and 48 h (1.14 ± 0.16). These findings indicate that the polymer was not completely eliminated from the body until that time point. Additionally, the ^{1}H/^{19}F-MR image overlay obtained 24 h post-injection (PI) clearly indicates that the fluorine signal originated from tumor tissue (Fig. 2a). Throughout the experiment, the fluorine signal remained higher than the phosphorus signal. Changes in ^{19}F- and ^{31}P-MRS SNR over time are depicted in Fig. 2b. A summary of the independent measurements, along with additional details and data, is provided in Supplementary Fig. 8. In summary, our results underscore the sufficient signal detection and localization of the ^{31}P/^{19}F-polymer using ^{31}P- and ^{19}F-MR techniques in vivo, even 48 h PI, highlighting the ROS-responsiveness of the dual polymer in the cancer tissue.

Discussion

In response to the gap in preclinical biocompatible and specific probes for X-nuclei MR in pathology, we investigated the MR properties of ROS-sensitive phospho-/fluoropolymers. Initially, in vitro experiments were conducted to establish baseline ROS production in cell cultures using fluorescent probes. Detecting ROS is challenging due to their low concentrations (often within the nanomolar range), short half-lives, and the impact of surrounding oxygen levels, which can trigger oxidative stress and structural changes[48]. Even atmospheric oxygen levels of 21% alone are capable of inducing oxidative stress without additional stimulation. However, physiological oxygen concentrations in the human body are much lower[49]. Therefore, it is feasible to measure ROS at lower oxygen concentrations. Signal fluctuations led to comparing several controls to accurately reflect probe oxidation. Future ROS measurements may benefit from atmospheric control units or bioreactors implementation.

ROS measurement in cell cultures is influenced by factors like spontaneous and H_2O_2-induced apoptosis, which vary with cell density[33]. Some researchers report on a linear increase in the rate of HO· production with rising cell density and normalize ROS levels to the number of viable cells[50], which could be tested in future ROS-production experiments, where additional information can be gained from varying cell densities. Additionally, nonadherent cell lines in suspension allow immediate probe application, whereas adherent cultures require an incubation time ranging from a few hours up to one day[33]. This factor was reflected in THP-1 cell line behavior, where cells enclosed in Eppendorf tubes with growth medium more closely resembled physiological conditions.

A comparison of ROS regulation in cancer vs. healthy cell lines was discussed in ref. 34, where it showed that cancer cells, whose antioxidant systems are already triggered, are more sensitive to ROS increases and are unable to achieve redox balance, leading to higher cancer cell death rates. Dead cells can also contribute to hypoxia, affecting the oxidation rate of P = S groups in the polymer probe. Furthermore, the increase in the phosphorus signal observed during our initial measurements may have reflected changes in MR properties, like relaxation times.

In prostate cancer cells (PC3, DU145, LNCaP) ROS generation is higher than in normal cells[51]. In our study, PC3 cells were used for in vitro MR of the responsive polymer, with H_2O_2 and NaClO as controls for hypoxic and inflammatory environments. As previously demonstrated, PC3 plays an essential role in ROS production through activation of NADPH oxidase (NOX), an extramitochondrial source involved in tumor progression and metastasis that can lead to ROS increase in the tumor microenvironment[38]. Elevated oxidative signaling in various type of cancers, including breast, pancreas, bladder, colon, lung, and prostate cancer, promotes tumor progression[52]. Furthermore, untreated tumors typically have very low oxygen levels, comparing to median oxygenation typically ranges between 3 and 7.4%, and exhibits oxygen levels between 0.3 and 4.2%, affecting ROS and polymer oxidation rates.

For ROS fluorescent detection, simple buffers, such as phosphate-buffered saline (PBS), Hanks' balanced salt solution (HBSS), or 4-(2-hydroxyethyl)−1-piperazineethanesulfonic acid (HEPES) are preferable over complex media. Additionally, a minimal loading dose is recommended to obtain a stronger fluorescence signal[33]. We used FluoroBrite DMEM, a specialized medium for extended optical measurements, to minimize the high impact of PBS on cell viability and without the addition of serum or phenol red achieve low background fluorescence[36].

Strict adherence to physiological conditions is crucial for cell viability in prolonged experiments. In this study, cell viability was assessed in Eppendorf tubes at room temperature, and remained high (>90%). In vitro ^{31}P-MR spectroscopy showed signal decay observed in normal cell lines, which may be attributed to the decline in culture viability over time, unlike resistant cancer cell lines. This phenomenon was evident even in prolonged measurements (>24 h), where the decline in the P = S signal was observed across all cell cultures.

Under model oxidative conditions with H_2O_2 or NaClO, the P = S phosphorus signal decreased rapidly due to high oxidation, contrasting with cell lines behavior. Quantification methods for MR signals were adapted for polymer structure changes, with P = S signals shifting to P = O, overlapping with physiological phosphorus signals[53,54]. Therefore, changes in signal amplitude under oxidizing conditions were quantified based on the P = S signal. Another reason for adopting this approach is the potential for the physiological P = O phosphorus signal to increase over time; spectral changes in adenosine triphosphate levels, for example, are associated with cell death[43]. In the case of the ^{31}P/^{19}F-polymer, fluorine signal remained unchanged under the influence of ROS over time, confirming polymer tracking using fluorine MRI and MRSI.

In vivo experiments used a copolymer comprising fluorine and phosphorus groups for dual ^{31}P/^{19}F-MR, allowing ROS triggered functionality assessment and provided an on-site reference for localization in the body. The exogenous probe precise localization and functionality, even at low concentrations in vivo, offers new opportunities for preclinical and clinical applications, such as is in theranostics, where phosphopolymers are covalently bound to antitumor drugs like 5-fluorouracil (5-FU), where therapeutic effects, biodistribution, and pharmacokinetics of the drug are simultaneously monitored using ^{31}P/^{19}F-MR in vivo (data not published). However, differences in ^{31}P-MRS amplitude of the physiological signal due to factors like hypoxia in the tumor and the loss of cells over time[55]. Therefore, signals within this frequency range can be challenging to quantify.

With these considerations in mind, we aim to obtain information from fluorine MR. The polymer's molecular weight (~17 kDa) facilitated tumor accumulation via the EPR effect, enhancing pharmacokinetics and ensuring excretion from the body post-task (the renal threshold for methacrylate-based polymers is ~45 kDa[56]). Biodistribution analysis confirmed that the length of the polymer chains enabled it to function effectively as a passive tumor-specific probe, remaining MR-detectable for up to two days. The increase in the signal observed after the retro-orbital injection is particularly encouraging, as it allows higher dosages and easier handling, deemed less stressful and more humane for the animals involved[57]. The higher signals observed after the I.T. injection are connected with the injection method, as both intravenous and intratumoral injections were measured at the same post-injection time points. Intravenous injections require more time for the polymer to passively accumulate and exhibit higher polymer dissolution within the system. Poor perfusion and elimination rates (after 24 h) can provide valuable insight for our future measurements, particularly as we aim to observe signal changes across various models and track the impact of attached drugs or ROS-based treatments on tumor size over time. Prolonged retention of the probe within the tumor allows for extended treatment duration and its biocompatibility ensures the safety of this system even during prolonged treatments. The I.T. injections in the long-term preclinical studies can serve as an indicator of the possible pathology onset with preferably I.V. injections used in the future and higher dosages.

The fluorine signal originating from the bladder and kidneys indicated polymer elimination from the body by day two post-injection. High ^{19}F-MRS signal amplitude observed 6 h PI in animals that received the retro-orbital injection indicates that the signal did not solely originate from the bladder (as visible in the MRI) but may have also originate from the tumor, where the signal is strongly suppressed. Six hour after intravenous injection, the MR signal was low and only slightly detectable in the kidney, indicating that the polymer had yet to accumulate in the tumor. An increase in the signal in both MRS and MRSI was detected only 48 h PI.

Our ongoing experimental work highlights the rapid polymer probe accumulation in tumors and high responsiveness. Pending confirmation of ROS-triggered signal changes in vivo, we expect to further test the dual ^{31}P/^{19}F-MR probe as an indicator of ROS levels in bacterial infections and cancer using different preclinical animal models and ultrahigh field MR. This probe could also be valuable for quantification ROS-based therapies in cancer treatment. The growing body of experimental data underscore the covert role of ROS generation in eliminating cancer cells via different metabolic pathways[34]. The ability of P = S groups to scavenge free radicals and their oxidation to form P = O groups[58–61] may have therapeutic effects on cancer and inflammation. In parallel, saturation of P = S groups of the polymer with free radicals over time can be detected using ^{31}P-MR. This property allows real-time in vivo imaging of the redox environment across clinically relevant imaging methods, demonstrating its utility in noninvasive imaging of ROS-rich pathologies, particularly in capturing the physiological and anatomical aspects of these conditions.

Methods

Chemicals

The compounds 2,2′-azobis(2-methylpropionitrile) (AIBN), 2-cyano-2-propyl benzodithioate (CPB), ethylene glycol, 4-methoxyphenol (MEHQ), thiophosphorylchloride, *N,N*'-dicyclohexylcarbodiimide (DCC), triethylamine (Et_3N), and 2-thiazoline-2-thiol (TT) were purchased from Sigma-Aldrich, Czech Republic. The chemicals 3-aminopropanoic acid, 3,5-bis(-trifluoromethyl)benzylamine (BTFBA), 2-hydroxyethyl methacrylate (HEMA), methacryloyl chloride, and trimethylamine (Me_3N) were purchased from TCI Europe, Belgium. All solvents (HPLC grade), obtained from VWR International, Czech Republic, were dried over a layer of activated molecular sieves (4 Å) before use.

Synthesis of monomers

Synthesis of TMPC was performed according to a previously described procedure by reacting thiophosphorylchloride with ethylene glycol to give 2-chloro-1,3,2-dioxaphospholane-2-thione, which further reacted with HEMA in the presence of Et_3N to form 2-((2-thioxo-1,3,2-dioxaphospholan-2-yl) oxy)ethyl methylmethacrylate. The resulting TMPC monomer was obtained by subsequently opening the phospholane ring of 2-((2-thioxo-1,3,2-dioxaphospholan-2-yl)oxy)ethyl methylmethacrylate with Me_3N[6]. Synthesis of 3-(3-methacrylamidopropanoyl)thiazolidine-2-thione (Ma-βAla-TT) was performed by acylating 3-aminopropanoic acid with methacryloyl chloride in an aqueous alkaline medium followed by the reaction of the formed 3-methacrylamidopropanoic acid with TT in the presence of DCC and DMAP, as described previously[62].

Synthesis of polymers

The polymer known as p(TMPC), hereafter referred to as the ^{31}P-polymer, was generated by RAFT polymerization of TMPC in the presence of CPB and AIBN in methanol at 60 °C for 16 h, as previously described[6]. The number-average molecular weight (M_n) and dispersity (Đ) of the polymer were 22.1 kg·mol^{-1} and 1.02, respectively. The polymer known as p(TMPC-*co*-Ma-βAla-BTFBA), hereafter referred to as the ^{31}P/^{19}F-polymer, was synthesized in three steps.

First, TMPC (2.0 g, 6.4 mmol) was dissolved in methanol (6 mL) and added to a mixture of CPB (37.5 mg, 0.17 mmol), AIBN (13.9 mg, 84.7 μmol), and Ma-βAla-TT (711.8 mg, 2.8 mmol) in dimethyl sulfoxide (4.2 mL). The polymerization mixture was thoroughly bubbled with argon and polymerized in a sealed glass ampoule at 70 °C for 16 h. After cooling to room temperature, the reaction mixture was precipitated into a 20-fold excess of acetone–diethyl ether (3:1) and reprecipitated from methanol into acetone. Centrifugation and vacuum drying of the precipitate afforded 1.23 g of the p(TMPC-*co*-Ma-βAla-TT)-DTB polymer precursor as an orange powder.

Second, a mixture of p(TMPC-*co*-Ma-βAla-TT)-DTB (350 mg, 28.2 μmol DTB groups) and AIBN (92.7 mg, 0.56 mmol) was dissolved in methanol (1.0 mL), thoroughly bubbled with argon, and incubated at 80 °C for 2 h. After cooling to room temperature, the reaction mixture was precipitated into a 20-fold excess of acetone–diethyl ether (3:1) and reprecipitated from methanol into acetone. Centrifugation and vacuum drying of the precipitate afforded 321 mg of the p(TMPC-*co*-Ma-βAla-TT) polymer precursor as a white powder. The M_n and $Đ$ of the polymer were 12.4 kg·mol^{-1} and 1.1, respectively. The molar content of the TT groups was 16 mol%.

Third, BTFBA (37.4 mg, 0.15 mmol) was dissolved in dimethyl sulfoxide (0.6 mL) and added to a solution of p(TMPC-*co*-Ma-βAla-TT) (291 mg, 0.15 mmol) in methanol (2.2 mL). The reaction mixture was incubated at room temperature overnight. After precipitation into a 20-fold excess of acetone–diethyl ether (3:1), the precipitate was dissolved in methanol and purified by gel filtration using a Sephadex LH-20 cartridge in methanol with 10 mM LiBr. The polymer was isolated by precipitation into acetone followed by centrifugation and vacuum drying to give 220 mg of p(TMPC-*co*-Ma-βAla-BTFBA) as a white powder. The M_n and $Đ$ of the polymer were 16.7 kg·mol^{-1} and 1.1, respectively. The molar content of the BTFBA groups was 15 mol%.

UV–visible spectrophotometry

Spectrophotometric analysis of the polymers was carried out in quartz glass cuvettes on a Specord Plus UV–vis spectrophotometer (Analytik Jena, Germany). The molar content of the terminal DTB groups and pendant TT groups in the polymers was determined in 1 cm quartz glass cuvettes at 302 nm and 305 nm at concentrations of 1.0 and 0.1 mg·mL^{-1} in methanol using a molar absorption coefficient of 12,100 and 10,300 L·mol^{-1}·cm^{-1}, respectively.

High-performance liquid chromatography

The purity of all low-molecular-weight compounds synthesized in this study was verified using a high-performance liquid chromatography (HPLC) system (Shimadzu, Japan) equipped with an internal UV–Vis diode array detector (SPD-M20A). Separation was performed using the Chromolith HighResolution RP18 endcapped reversed-phase column (Merck, USA) with a linear gradient (0–100%) of a water–acetonitrile mixture containing 0.1% TFA at a flow rate of 2.5 mL·min^{-1}.

Size exclusion chromatography

The number-average molecular weight, weight-average molecular weight (M_n and M_w), and dispersities ($Đ^{SEC}$, $Đ^{SEC} = M_w/M_n$) of TMPC-based polymers were determined by size exclusion chromatography using a HPLC system (Shimadzu, Japan) equipped with an internal UV–Vis diode array detector (SPD-M20A), an external differential refractometer (Optilab T-rEX), and a multiangle light-scattering detector (DAWN HELEOS II, both Wyatt Technology, USA). TSK gel SuperAW3000 and SuperAW4000 columns (Tosoh Bioscience, USA) were used in series to analyze samples in a mobile phase of 80% methanol and 20% sodium acetate buffer (0.3 M, pH 6.5) at a flow rate of 0.6 mL·min^{-1}. The d*n*/d*c* values of 0.125 mL·g^{-1} were used to calculate the molecular weights of the TMPC-based polymers.

NMR spectroscopy

The composition of polymers was determined by ^{1}H-, ^{31}P-, and ^{19}F-NMR spectroscopy in deuterated solvents at 25 °C on a Bruker NEO spectrometer (Bruker, MA, USA) operating at 400, 376.48, and 161.97 MHz for ^{1}H, ^{19}F, and ^{31}P, respectively. ^{1}H-NMR spectra were calibrated to the signal of the internal standard tetramethylsilane (TMS) at $\delta = 0.00$ MHz. Typical measurement conditions were as follows: ^{1}H NMR: "zg" pulse sequence, π/2 pulse width 16.5 µs, relaxation delay 10 s, spectral width 12 kHz, scan time 2.75 s, 32 scans. ^{19}F NMR: "zg" pulse sequence, π/2 pulse width 19 µs, relaxation delay 3 s, spectral width 37 kHz, scan time 0.20 s, 128 scans. ^{31}P NMR: "zgpg" pulse sequence, π/2 pulse width 10 µs, relaxation delay 3 s, spectral width 71 kHz, scan time 2.99 s, 500 scans.

Cell lines

Cell lines were purchased from American Type Culture Collection® (Manassas, VA, USA). The PC3 cells were cultured in Dulbecco's modified Eagle's medium (DMEM) supplemented with Ham's F-12 nutrient mixture (Gibco, Thermo Fisher Scientific, USA), 1% GlutaMAX (Gibco, Thermo Fisher Scientific, USA), 10% fetal bovine serum (FBS, Gibco, Thermo Fisher Scientific, USA), and 1% penicillin–streptomycin (Biosera, France). The 4T1, THP-1, and RAW 264.7 cell lines were cultured in RPMI 1640 media (Gibco, Thermo Fisher Scientific) supplemented with 2 mmol L^{-1} L-glutamine, 10% FBS, and 1% penicillin–streptomycin. All cells were incubated under standard conditions ($T = 37$ °C; 5% CO_2).

ROS production under hypoxic conditions. To investigate extracellular ROS production, we employed 4T1 cancer cell line, as an in vitro model representing ROS-rich tissue. The cell line was cultured as described in the previous section. The 4T1 cell line was selected and tested for its relevance in an in vivo cancer model. For live-cell imaging, cells were seeded in a 96-well plate (2×10^6 mL^{-1}) and incubated for 24 h. Subsequently, the cells were washed three times with phosphate-buffered saline (PBS, Gibco, Thermo Fisher Scientific) before changing the medium for FluoroBrite DMEM (Gibco, Thermo Fisher Scientific) containing 10 µmol L^{-1} OB (Invitrogen, Thermo Fisher Scientific, USA) in triplicate. FluoroBrite DMEM was used in all measurements because it exhibits no background fluorescence. OB is a sensitive fluorogenic reagent that detects the extracellular release of oxidative products. Excited at 488 nm and emitted at 530 nm, the fluorescent product is formed by oxidation of the nonfluorescent substrate, where the rate of fluorescence increase is proportional to the number of oxidative species generated. The signal was detected using a fluorescence optical imager (AMI HT, Spectral Instruments, USA).

In order to establish the production of ROS within the cell line, both positive (using OB dye with 50 nM to 1 µM H_2O_2 range) and negative (using OB dye alone) controls were implemented. Additionally, hydrogen peroxide, at concentrations ranging from 50 nM to 1 µM, was introduced to the cells, dye, and culture medium to act as a positive control for measurement. Cellular imaging was conducted at various intervals over an 8-h period following staining. Image analysis and signal quantification were performed using ImageJ 1.48 (National Institutes of Health, Bethesda, USA) and Aura 4.0 (Spectral Imaging, USA) software, whereby the signal intensity was measured as the total emission (photons per second) within the designated region of interest (ROI). This measurement was repeated three times for each time point, and the ratio of signal intensity between the experimental and control groups was plotted against time.

MR instrumentation

MR experiments were performed employing the BioSpec 47/20 preclinical experimental 4.7 T and 14.1 T scanners (Bruker, Ettlingen, Germany). On 4.7 T scanner, characterization of the polymer was performed using a small, highly sensitive radiofrequency (RF) solenoid coil customized for ^{1}H-, ^{19}F-, and ^{31}P-MR spectroscopy (diameter = 8 mm, length = 8 mm, 4 turns)[4]. The resonance frequency was continuously adjustable within a range of 80 to 210 MHz, corresponding to the respective Larmor frequencies of the ^{31}P (81 MHz), ^{19}F (188 MHz), and ^{1}H (200 MHz) nuclei. This coil, due to its exceptional sensitivity and the small probe volume ($V = 0.5$ mL) required for high-quality ^{31}P-MR signal quantification, was also deemed suitable for in vitro measurement of the polymer under oxidative conditions.

Measurements, which involved ^{1}H-MR imaging, ^{19}F-MR spectroscopy and imaging, and ^{31}P-MR spectroscopy, were conducted using a combination of two surface RF coils. For anatomy analysis (^{1}H-MRI) and probe localization (^{19}F-MRI), a custom dual ^{1}H/^{19}F coil (diameter = 40 mm) designed for continuous tuning between ^{1}H and ^{19}F Larmor frequencies was utilized. The second coil (diameter = 30 mm), a rectangular half-saddle model optimized for in vivo mouse experiments, was used for ^{31}P-MR measurements.

Additional measurements of the probe internalization were made using 14.1 T MR scanner with ^{1}H/^{19}F volume coil. The signal sensitivity of the probe on lower magnetic fields was measured using 3.0 T clinical MR scanner, and 7 T experimental MR scanner was used to confirm the phosphorus signal-detectability in vivo; in both systems commercial surface ^{1}H/^{31}P coils were used.

MR of the ^{31}P-polymer under hypoxic conditions

In a previous study, we employed ^{31}P-MRS alongside a combination of ^{1}H- and ^{31}P-MRI techniques to characterize a phosphorus-based ^{31}P-polymer, determining its relaxivity and sensitivity. Furthermore, cytotoxicity testing of the polymer was conducted prior to in vivo measurement, revealing no toxic effects on the viability of two distinct cell cultures[6]. Herein, the oxidation of the ^{31}P-polymer in vitro was tested to evaluate its sensitivity for ^{31}P-MR signal changes using an RF solenoid coil. We investigated ROS-triggered chemical shift of the polymer under various oxidative conditions. For this investigation, we used the ^{31}P-polymer containing solely the phosphorus P = S groups, as the simplicity of the cell line-based model does not require biodistribution monitoring. ^{31}P-MR spectroscopy was performed using a single-pulse sequence (repetition time TR = 500 ms, ST = 5 min, bandwidth BW = 200 ppm) over a prolonged period of up to 24 h.

Initially, the ^{31}P-polymer ($c^P = 10$ mmol L^{-1}; $V = 0.4$ mL in dH_2O) was mixed with either H_2O_2 ($c = 20$ mmol L^{-1}; mimicking hypoxic tumor tissue) or NaClO ($c = 20$ mmol L^{-1}; mimicking bacterial inflammation). Subsequently, the same MR measurements were proceeded with the polymer ($c^P = 10$ mmol L^{-1}; $V = 0.05$ mL in PBS) added to a suspension of 4T1, PC3, and THP-1 cancer cell lines (average of 106.3×10^6 mL^{-1}, with $V = 0.35$ mL of the respective cells in cell culture media). To prevent the creation of a strongly hypoxic environment, all cell measurements were performed in microcentrifuge tubes ($V = 0.5$ mL) with a sterile syringe filter (Ø 4 mm; 0.2-µm pore size; BRAND, Merck Life Science, Germany) securely attached to the tube's top. The filter ensured aseptic conditions throughout the measurement while allowing for air exchange. Additionally, to exclude the influence of autoxidation, the polymer was measured in the cell-free culture medium under identical conditions ($c^P = 10$ mmol L^{-1}; $V = 0.4$ mL).

For the in vitro experimental setup, we used the ^{31}P-polymer polymer carrying solely the phosphorus P = S groups, as biodistribution data were not required. Localization was measured using ^{1}H-MR imaging employing a rapid acquisition with relaxation enhancement (RARE) sequence. Samples from the PC3 cell line were incubated in Eppendorf tubes at room temperature for subsequent measurements. Cell viability was assessed at three time points within 1 to 3 h of incubation utilizing an automated cell counter. The phosphorus-based probe relaxation times and MR parameters were based on results from our previous study (ref. 6): ^{1}H-MR $T_1/T_2 = 2510.0/2067.2$ ms, ^{31}P-MR $T_1/T_2 = 2018.3/119.9$ ms.

The sensitivity of the ^{31}P-polymer ($c^P = 100$ mmol L^{-1}; $V = 1.5$ mL) and responsiveness to the ROS-rich environment (H_2O_2, $V = 100$ µL) was further tested on the clinical 3 T MR scanner using ^{31}P-MR spectroscopy (single-pulse sequence, TR = 1000 ms, ST = 8 min, BW = 140 ppm). The measurements were done right after the addition of the H_2O_2 and after 24 h.

MR sensitivity and responsiveness of the dual $^{31}P/^{19}F$-Polymer

A newly synthesized double $^{31}P/^{19}F$-polymer was measured to validate the sensitivity, responsiveness, and stability of both phosphorus and fluorine signals under hypoxic conditions. The probe ($c^{P} = 10$ mmol L^{-1}; $V = 0.4$ mL in dH_2O) underwent initial measurement using $^{31}P/^{19}F$-MRS (^{19}F: single-pulse sequence; TR = 500 ms, ST = 5 min, BW = 40 ppm; ^{31}P: single-pulse sequence; TR = 200 ms, ST = 10 min, BW = 200 ppm). To confirm the chemical shift in both fluorine and phosphorus MR, the polymer was measured using ^{19}F-MRSI (chemical shift imaging CSI sequence; TR = 200 ms, FOV = 35 × 35 mm, slice thickness = 10 mm, ST = 6–30 min) and ^{31}P-MRSI (CSI sequence; TR = 200 ms, FOV = 35 × 35 mm, slice thickness = 10 mm, ST = 6–30 min) alongside ^{1}H-MRI reference images (^{1}H: RARE sequence, coronal plane, TR/echo time TE = 3300/11.7 ms, field of view FOV = 35 × 35 mm, slice thickness = 0.6 mm, ST = 5 m 16 s). Sensitivity was established based on repeat MRSI measurements with varying scan times. Finally, the polymer was measured with hydrogen peroxide (H_2O_2; $c = 20$ mmol L^{-1}) to establish its responsiveness under hypoxic conditions compared to the ^{31}P-polymer and the stability of the fluorine signal over a period of 24 h.

Additionally, $^{31}P/^{19}F$-polymer ($c^{P} = 10$ mmol L^{-1}; $V = 0.4$ mL in dH_2O) tested for cell (RAW264.7) internalization was measured using standard ^{1}H-MRI reference images, ^{19}F-MRS single-pulse sequence (only polymer; TR = 1000 ms, ST = 2 min 30 s, BW = 200 ppm) and ^{19}F-MRS Point-RESolved Spectroscopy sequence (PRESS, TR = 1000 ms, ST = 1 h, BW = 50 ppm; polymer mixed with H_2O_2, cells treated with the polymer and the control cells).

In vivo MR

Animal protocols were approved by the Ethics Committee of the Institute for Clinical and Experimental Medicine and the Ministry of Health of the Czech Republic (No. 58/2014) in accordance with the European Communities Council Directive (2010/63/EU). Animals, provided by Animalab (Czech Republic), were housed in standard laboratory cages with a 12-h light–dark cycle in a conventional breeding facility, with ad libitum access to water and pelleted food. Isoflurane (Baxter, Deerfield, USA) was administrated for anesthesia during injections and MR experiments (5% for induction, 1.5 to 2% for maintenance). Respiratory function was monitored using a trigger unit (Rapid Biomedical, Berlin, Germany), and eye cream (Ophthalmo-Septonex, Zentiva, Czech Republic) was applied to prevent eye dryness. During MR measurements, animals were positioned in a custom coil holder heated with water-filled tubes to maintain a temperature of 37 °C.

To induce tumor growth in vivo, a cell suspension (0.5×10^{6} 4T1 cells; $V = 0.1$ mL in PBS) was subcutaneously injected into the right mammary fat pad of healthy female Balb/c mice. Animals were monitored daily once tumor volume exceeded 1 mL. For polymer biodistribution experiments (see section *Proof-of-Principle* In Vivo *Biodistribution Based on ^{19}F-MR*), mice received I.V. injections ($V = 0.15$ mL in PBS) via the lateral tail vein or retro-orbitally via the venous sinus ($V = 0.2$ mL in PBS). In dual $^{31}P/^{19}F$-MR experiments (see section *MR Sensitivity and Responsiveness of the dual $^{31}P/^{19}F$-Polymer*), animals received I.T. injection of the polymer ($^{31}P/^{19}F$-polymer; $c^{P} = 100$ mmol L^{-1}; $c^{F} = 112.5$ mmol L^{-1}) to determine the influence of ROS on the probe. For all in vivo experiments, an aqueous solution of the polymer was injected.

Proof-of-principle in vivo biodistribution based on ^{19}F-MR. In vivo investigations aimed to assess the biodistribution and efficiency of the $^{31}P/^{19}F$-polymer in reaching the tumor via passive accumulation. Leveraging the EPR effect, inherent to tumors with compromised lymphatic drainage, these studies were conducted on Balb/c mice bearing established tumors. Injections were administrated at two different sites to evaluate delivery efficiency. Comparison between intravenous I.V. and R.O. injection methods were performed using the dual $^{31}P/^{19}F$-polymer ($V = 0.15$ / 0.2 mL in PBS, respectively). Monitoring of the animals employed several MR methods, with the highly sensitive fluorine signal used as the distribution indicator. These techniques included ^{1}H-MR imaging (RARE sequence, coronal plane, TR/TE = 3300/11.7 ms, FOV = 60 × 60 mm, slice thickness = 1.2 mm, ST = 1 m 19 s), ^{19}F-MR spectroscopy (single-pulse sequence; TR = 150 ms, ST = 5 min, BW = 100 ppm), and ^{19}F-MR imaging (CSI; TR = 150 ms, ST = 10–120 min, BW = 100 ppm). The dual $^{1}H/^{19}F$ RF surface coil was positioned beneath the tumor site. MR measurements were obtained at three time points: 6 h (day 0 + 6 h), followed by 24 h (day 1, R.O. injection) and 48 h (day 2, I.V. injection) PI.

Dual $^{31}P/^{19}F$ in vivo MR under hypoxic conditions. Animal monitoring was conducted daily throughout the study. Once tumor volume reached 1.6 ± 0.6 mL, animals ($N = 5$) received an I.T. injections of the $^{31}P/^{19}F$-polymer ($V = 0.2$ mL in PBS). To investigate ROS-triggered chemical shifts and to track polymer degradation in vivo, three MR methods were used: ^{1}H-MR imaging (RARE sequence, coronal plane, TR/TE = 3300/11.7 ms, FOV = 40 × 40 mm, slice thickness = 1.3 mm, ST = 1 m 19 s), $^{31}P/^{19}F$-MR spectroscopy (single-pulse sequence; TR = 200/500 ms, ST = 10/5 min, BW = 200/40 ppm), and ^{19}F-MR imaging (CSI; TR = 200 ms, ST = 1 h 8 m, BW = 40 ppm). Initially, the dual $^{1}H/^{19}F$ RF surface coil was positioned beneath the tumor site. Subsequently, it was replaced with a phosphorus RF surface coil while maintaining the same animal holder to ensure data repeatability. MR measurements were performed immediately after injection ($t = 0.5$ h) and repeated at 24- and 48-h PI.

Quantification of MR imaging and spectroscopy data

Data processing and quantification for both $^{31}P/^{19}F$-MR spectroscopy and $^{1}H/^{19}F$-MR imaging was primarily carried out using custom-written scripts developed in Matlab (Matlab R2021b, MathWorks, USA). The scripts facilitated the simultaneous processing of time series data, including nonlocalized measurements. Peak amplitude (for in vitro data) or integral (for in vivo data) was used to determine the relative concentration of ^{31}P nuclei (P = S signal, with a chemical shift of Δδ ~ 60 ppm from the physiological signal) or fluorine signal (CF_3 signal, with a chemical shift of Δδ ~ 20 ppm from the isoflurane). The same ppm range was applied for both signal and noise calculations. Apodization techniques were not applied during quantification to avoid potential spectral distortion. Evaluation of in vivo "hotspot" ^{19}F-CSI sequences involved identifying the resonance frequency range of fluorine, employing matrix normalization to enhance contrast in the reconstructed CSI image, suppressing the background noise, and overlaying the ^{1}H-MRI reference and ^{19}F-CSI image. For extended in vitro measurements, the ^{31}P-MRS signal was averaged over each hour of the experiment and expressed as a percentage change in signal amplitude relative to the experiment onset. In vivo ^{19}F- and ^{31}P-MRS data were quantified using an integral (I) ratio of signal (S) and noise (N), calculated as $SNR_{MRS} = \frac{S_I}{N_I}$ (1). Due to the overlapping frequencies of the physiological phosphorus signal (81.157 kHz), quantification of the total conversion of the phosphorus signal to the P = O groups was not feasible. Instead, the amplitude or integral of the P = S phosphorus MR signal was evaluated. Quantification of the ^{19}F-CSI signal and background noise was performed using ImageJ software, and the SNR was calculated as $SNR_{MRI} = \frac{S}{\sigma_s} \cdot 0.655$ (2), where S is the signal intensity in ROI, σ is the standard deviation of background noise, and the constant 0.655 accounts for the Rician distribution of background noise in the magnitude MR image[63].

Conclusion

This study introduces ROS-sensitive probes derived from hydrophilic phospho-/fluoropolymers for application in X-nuclei MR. Our results demonstrate their reliable monitoring via $^{31}P/^{19}F$-MR techniques, serving as sensitive ^{31}P-MR sensors capable of detecting ROS overproduction in specific pathologies, observed even at magnetic field strengths used in clinical practice. The probe's design includes a thiophosphoester groups (P = S), which exhibits a distinct chemical shift relative to signals from naturally occurring biomolecules, making it detectable in vivo. The P = S groups acts as an in situ ROS detector, with oxidation leading to a detectable ^{31}P-MR chemical shift change. Furthermore, the incorporation of a trifluoromethyl groups (CF_3) aids in localizing the probe by ^{19}F-MR, offering precise on-site information regarding pharmacokinetics and distribution data within the body with high specificity, reaching 100%.

Our findings highlight the probe's accumulation at tumor sites and its in vivo responsiveness, as indicated by natural clearance and ROS-induced oxidation. The MR-based localization and functionality of this exogenous probe, even at low concentrations in vivo, show promise as a versatile tool for functional and on-site localization using ^{31}P/^{19}F-MR imaging. With unique properties including distinct chemical shifts, ROS scavenging capabilities, and biodistribution tracking, this probe holds significant potential for elucidating oxidative stress's role in disease and exploring targeted therapeutic ROS-based interventions. Consequently, it represents an innovative approach to responsive ^{31}P-MR, complementing traditional ^{1}H-MRI anatomical information by providing insights into tumor physiology.

Reporting summary

Further information on research design is available in the Nature Portfolio Reporting Summary linked to this article.

Data availability

The datasets generated during and/or analysed during the current study are available from the corresponding author on reasonable request.

Code availability

The custom-written scripts generated for MR data analyses developed in Matlab (Matlab R2021b, MathWorks, USA) during the current study are available from the corresponding author on reasonable request.

Received: 29 February 2024; Accepted: 23 August 2024;
Published online: 05 September 2024

References

1. Pasquini, L. et al. Gadolinium-based contrast agent-related toxicities. *CNS Drugs* **32**, 229–240 (2018).
2. Sedlacek, O. et al. Fluorinated water-soluble Poly(2-oxazoline)s as highly sensitive 19F MRI contrast agents. *Macromolecules* **53**, 6387–6395 (2020).
3. Kolouchova, K. et al. Implant-forming polymeric 19F MRI-tracer with tunable dissolution. *J. Control. Release* **327**, 50–60 (2020).
4. Ziółkowska, N., Vít, M., Laga, R. & Jirak, D. Iron-doped calcium phytate nanoparticles as a bio-responsive contrast agent in ^{1}H/^{31}P magnetic resonance imaging. *Sci. Rep.* **12**, 2118 (2022).
5. Kracíková, L. et al. Iron-based compounds coordinated with phospho-polymers as biocompatible probes for dual 31P/1H magnetic resonance imaging and spectroscopy. *Sci. Rep.* **14**, 3847 (2024).
6. Kracíková, L. et al. Phosphorus-containing polymeric zwitterion: a pioneering bioresponsive probe for 31P-magnetic resonance imaging. *Macromol. Biosci.* **22**, 2100523 (2022).
7. Kolouchova, K. et al. Self-assembled thermoresponsive polymeric nanogels for 19F MR imaging. *Biomacromolecules* **19**, 3515–3524 (2018).
8. Sedlacek, O. et al. 19F Magnetic resonance imaging of injectable polymeric implants with multiresponsive behavior. *Chem. Mater.* **30**, 4892–4896 (2018).
9. Kolouchova, K. et al. Thermo- and ROS-responsive self-assembled polymer nanoparticle tracers for 19F MRI theranostics. *Biomacromolecules* **22**, 2325–2337 (2021).
10. Jirát-Ziółkowska, N. et al. Long-term in vivo dissolution of thermo- and pH-responsive, 19F magnetic resonance-traceable and injectable polymer implants. *Nanoscale Adv.* 6, 3041–3051 (2024).
11. Galisova, A. et al. A trimodal imaging platform for tracking viable transplanted pancreatic islets in vivo: F-19 MR, fluorescence, and bioluminescence imaging. *Mol. Imaging Biol.* **21**, 454–464 (2019).
12. Srinivas, M., Heerschap, A., Ahrens, E. T., Figdor, C. G. & de Vries, I. J. 19F MRI for quantitative in vivo cell tracking. *Trends Biotec.* **28**, 363–370 (2010).
13. Mali, A., Kaijzel, E. L., Lamb, H. J. & Cruz, L. J. 19F-nanoparticles: platform for in vivo delivery of fluorinated biomaterials for 19F-MRI. *J. Control. Release* **338**, 870–889 (2021).
14. Starke, L. et al. First in vivo fluorine-19 magnetic resonance imaging of the multiple sclerosis drug siponimod. *Theranostics* **13**, 1217–1234 (2023).
15. Gupta, A. Cardiac ^{31}P MR spectroscopy: development of the past five decades and future vision-will it be of diagnostic use in clinics? *Heart Fail. Rev.* **28**, 485–532 (2023).
16. Sedivy, P. et al. MR compatible ergometers for dynamic 31P MRS. *J. Appl. Biomed.* **17**, 91–98 (2019).
17. Valkovič, L., Chmelík, M. & Krššák, M. In-vivo31P-MRS of skeletal muscle and liver: a way for non-invasive assessment of their metabolism. *Anal. Biochem.* **529**, 193–215 (2017).
18. Podo, F. Tumour phospholipid metabolism. *NMR Biomed.* **12**, 413–439 (1999).
19. Ng, T. C. et al. Response of a non-Hodgkin lymphoma to 60Co therapy monitored by 31P MRS in situ. *Int. J. Radiat. Oncol. Biol. Phys.* **13**, 1545–1551 (1987).
20. Taylor, D. J. Clinical utility of muscle mr spectroscopy. *Semin. Musculoskelet. Radio.* **4**, 481–502 (2000).
21. McCoy, C. L., McIntyre, D. J. O., Robinson, S. P., Aboagye, E. O. & Griffiths, J. R. Magnetic resonance spectroscopy and imaging methods for measuring tumour and tissue oxygenation. *Br. J. Cancer* **74**, 231 (1996).
22. Kalra, R. et al. Phosphomonoester is associated with proliferation in human breast cancer: a 31P MRS study. *Br. J. Cancer* **67**, 1145–1153 (1993).
23. Jirak, D., Galisova, A., Kolouchova, K., Babuka, D. & Hruby, M. Fluorine polymer probes for magnetic resonance imaging: quo vadis?. *MGMA* **32**, 173–185 (2019).
24. Koshkina, O. et al. Biodegradable polyphosphoester micelles act as both background-free ^{31}P magnetic resonance imaging agents and drug nanocarriers. *Nat. Commun.* **14**, 4351 (2023).
25. Havlicek, D., Panakkal, V. M., Voska, L., Sedlacek, O. & Jirak, D. Self-assembled fluorinated nanoparticles as sensitive and biocompatible theranostic platforms for 19F MRI. macromolecular bioscience. *Macromol. Biosci.* **24**, e2300510 (2024).
26. Kohler, G. & Milstein, C. Continuous cultures of fused cells secreting antibody of predefined specificity. *Nature* **256**, 495–497 (1975).
27. Takakura, Y. & Hashida, M. Macromolecular drug carrier systems in cancer chemotherapy: macromolecular prodrugs. *Crit. Rev. Oncol. Hematol.* **18**, 207–231 (1995).
28. Maeda, H. The enhanced permeability and retention (EPR) effect in tumour vasculature: the key role of tumour-selective macromolecular drug targeting. *Adv. Enzym. Regul.* **41**, 189–201 (2001).
29. Zhang, Y. et al. Reactive oxygen species-responsive polymeric prodrug nanoparticles for selective and effective treatment of inflammatory diseases. *Adv. Healthc. Mater.* **12**, e2301394 (2023).
30. Zhang, S. et al. Preparation of Poly(bis(phenoxy)phosphazene) and 31P nmr analysis of its structural defects under various synthesis conditions. *J. Phys. Chem. B* **120**, 11307–11316 (2016).

31. Weikel, A. L., Owens, S. G., Fushimi, T. & Allcock, H. R. Synthesis and characterization of methionine- and cysteine-substituted phosphazenes. *Macromolecules* **43**, 5205–5210 (2010).
32. Kumar, A. et al. Kinetics of bacterial inactivation by 405 nm and 520 nm light emitting diodes and the role of endogenous coproporphyrin on bacterial susceptibility. *J. Photochem. Photobiol. B Biol.* **149**, 37–44 (2015).
33. Yazdani, M. Concerns in the application of fluorescent probes DCDHF-DA, DHR 123 and DHE to measure reactive oxygen species in vitro. *Toxicol. Vitr.* **30**, 578–582 (2015).
34. Perillo, B. et al. ROS in cancer therapy: the bright side of the moon. *Exp. Mol. Med.* **52**, 192–203 (2020).
35. Juan, C. A., Pérez de la Lastra, J. M., Plou, F. J. & Pérez-Lebeña, E. The chemistry of reactive oxygen species (ROS) Revisited: outlining their role in biological macromolecules (DNA, Lipids and Proteins) and induced pathologies. *Int. J. Mol. Sci.* **22**, 4642 (2021).
36. Zhang, X. & Soldati, T. Detecting, visualizing and quantitating the generation of reactive oxygen species in an amoeba model system. *J. Vis. Exp.* **81**, e50717 (2013).
37. Lim, H.-W. et al. Up-regulation of defense enzymes is responsible for low reactive oxygen species in malignant prostate cancer cells. *Exp. Mol. Med.* **37**, 497–506 (2005).
38. Sankaralingam, S., Kumar, B., Shishodia, G., Koul, S. & Koul, H. Reactive oxygen species and cancer: a complex interaction. *Cancer Lett.* **452**, 132–143 (2019).
39. Galadari, S., Rahman, A., Pallichankandy, S. & Thayyullathil, F. Reactive oxygen species and cancer paradox: To promote or to suppress? *Free Radic. Biol. Med.* **104**, 144–164 (2017).
40. Wang, J. et al. Gossypol induces apoptosis in ovarian cancer cells through oxidative stress. *Mol. Biosyst.* **9**, 1489 (2013).
41. Huang, G. & Pan, S.-T. ROS-mediated therapeutic strategy in chemo-/radiotherapy of head and neck cancer. *Oxid. Med. Cell. Longev.* **2020**, 5047987 (2020).
42. Ikawa, M., Okazawa, H. & Yoneda, M. Molecular imaging for mitochondrial metabolism and oxidative stress in mitochondrial diseases and neurodegenerative disorders. *Biochim. et Biophys. Acta. Gen. Subj.* **1865**, 129832 (2021).
43. Okazawa, H., Ikawa, M., Tsujikawa, T., Kiyono, Y. & Yoneda, M. Brain imaging for oxidative stress and mitochondrial dysfunction in neurodegenerative diseases. *Q. J. Nucl. Med. Mol. Imaging.* **58**, 387–397 (2014).
44. Tsuchida, K., & Kobayashi, M. Oxidative stress in human facial skin observed by ultraweak photon emission imaging and its correlation with biophysical properties of skin. *Int. J. Mol. Sci.* **24,** 9626 (2020).
45. Mantri, Y., Davidi, B., Lemaster, J. E., Hariri, A. & Jokerst, J. V. Iodide-doped precious metal nanoparticles: measuring oxidative stress in vivo via photoacoustic imaging. *Nanoscale* **12**, 10511–10520 (2020).
46. Perng, J. K. et al. Ultrasound imaging of oxidative stress in vivo with chemically-generated gas microbubbles. *Ann. Biomed. Eng.* **40**, 2059–2068 (2012).
47. Espinoza, E. M., Røise, J. J., Li, I. C., Das, R. & Murthy, N. Advances in imaging reactive oxygen species. *J. Nucl. Med. Publ. Soc. Nucl. Med.* **62**, 457–461 (2021).
48. Katerji, M., Filippova, M. & Duerksen-Hughes, P. Approaches and methods to measure oxidative stress in clinical samples: research applications in the cancer field. *Oxid. Med. Cell. Longev.* **2019**, 1279250 (2019).
49. McKeown, S. R. Defining normoxia, physoxia and hypoxia in tumours-implications for treatment response. *Br. J. Radiol.* **87**, 20130676 (2014).
50. Bopp, S. K., Abicht, H. K. & Knauer, K. Copper-induced oxidative stress in rainbow trout gill cells. *Aquat. Toxicol.* **86**, 197–204 (2008).
51. Kumar, B., Koul, S., Khandrika, L., Meacham, R. B. & Koul, H. K. Oxidative stress is inherent in prostate cancer cells and is required for aggressive phenotype. *Cancer Res.* **68**, 1777–1785 (2008).
52. Prasad, S., Gupta, S. C. & Tyagi, A. K. Reactive oxygen species (ROS) and cancer: role of antioxidative nutraceuticals. *Cancer Lett.* **387**, 95–105 (2017).
53. Rothe, M., et al In vivo absolute quantification of hepatic γ-ATP concentration in mice using 31P MRS at 11.7 T. *NMR Biomed*. **34**, e4422 (2020).
54. Menon, Xia, D., Katz, S. D. & Regatte, R. R. Dynamic 31P-MRI and 31P-MRS of lower leg muscles in heart failure patients. *Sci. Rep.* **11**, 7412 (2021).
55. Tozer, G. M. & Griffiths, J. R. The contribution made by cell death and oxygenation to 31P MRS observations of tumour energy metabolism. *NMR Biomed.* **5**, 279–289 (1992).
56. Kostka, L. & Etrych, T. High-Molecular-Weight HPMA-Based Polymer Drug Carriers for Delivery to Tumor. *Physiol. Res.* **65**, 179–190 (2016).
57. Yardeni, T., Eckhaus, M., Morris, H. D., Huizing, M. & Hoogstraten-Miller, S. Retro-orbital injections in mice.*Lab. Anim.* **40**, 155–60 (2011).
58. Wu, T. et al. Mechanistic investigation on ROS resistance of phosphorothioated DNA. *Sci. Rep.* **7**, 42823 (2017).
59. Yang, N., Xiao, W., Song, X., Wang, W. & Dong, X. Recent advances in tumor microenvironment hydrogen peroxide-responsive materials for cancer photodynamic therapy. *Nanomicro. Lett.* **12**, 1–27 (2020).
60. Liu, J. et al. Biomedical application of reactive oxygen species–responsive nanocarriers in cancer, inflammation, and neurodegenerative diseases. *Front. Chem.* **8**, 838 (2020).
61. Vorobjeva, N. V. & Chernyak, B. V. NETosis: molecular mechanisms, role in physiology and pathology. *Biochem. Mosc.* **85**, 1178–1190 (2020).
62. Šubr, V. & Ulbrich, K. Synthesis and properties of new N-(2-hydroxypropyl)methacrylamide copolymers containing thiazolidine-2-thione reactive groups. *React. Funct. Polym.* **66**, 1525–1538 (2006).
63. Vit, M., Marton, P., Burian, M., Galisova, A. & Jirak, D. Construction of wide tuneable volume radiofrekvency coil for MR imaging of small rodents. *Ceska Radiologie* **72**, 1 (2018).

Acknowledgements

This work was supported by the National Institute for Research of Metabolic and Cardiovascular Diseases [Program EXCELES, Project no. LX22NPO5104] founded by the European Union – Next Generation EU program and the Ministry of Health of the Czech Republic [project no. MH CZ-DRO, Institute for Clinical and Experimental Medicine IKEM, IN 00023001], National Institute for Cancer Research (Program EXCELES, Project No. LX22NPO5102)-Funded by the European Union—Next Generation EU. We thank to Prof. Mangala Srinivas, Ph.D. (Department of Cell Biology and Immunology, Wageningen University & Research, Wageningen, The Netherlands) for providing access to the 14 T scanner and her group member Mariah Daal, MSc for technical assistance with MR experiments. Parts of the Figures presented in the Manuscript were created in BioRender.com. All data supporting the findings of this study are available within the paper and its Supplementary Information.

Author contributions

Natalia Jirát-Ziółkowska: Conceptualization, Data curation, Formal analysis, Investigation, Methodology, Visualization, Writing—Original Draft. Kateřina Sulková: Investigation, Formal analysis, Methodology. Lucie Kracíková: Formal analysis, Methodology, Investigation, Writing - Review & Editing, Visualization. Ladislav Androvič: Methodology, Writing—Review & Editing. Dominik Havliček: Formal analysis, Software. Richard Laga: Conceptualization, Methodology, Supervision, Writing—Original Draft. Daniel Jirák: Conceptualization, Supervision, Resources, Project administration, Funding acquisition, Writing—Original Draft.

Competing interests

The authors declare no competing interests.

Additional information

Supplementary information The online version contains supplementary material available at https://doi.org/10.1038/s43246-024-00623-z.

Correspondence and requests for materials should be addressed to Daniel Jirák.

Peer review information *Communications* Materials thanks Zuhir Elkarghali, Olga Koshkina and the other anonymous reviewer(s) for their contribution to the peer review of this work. Handling Editors: Daniela Loessner and Jet-Sing Lee

Reprints and permissions information is available at http://www.nature.com/reprints

Publisher's note Springer Nature remains neutral with regard to jurisdictional claims in published maps and institutional affiliations.

Open Access This article is licensed under a Creative Commons Attribution 4.0 International License, which permits use, sharing, adaptation, distribution and reproduction in any medium or format, as long as you give appropriate credit to the original author(s) and the source, provide a link to the Creative Commons licence, and indicate if changes were made. The images or other third party material in this article are included in the article's Creative Commons licence, unless indicated otherwise in a credit line to the material. If material is not included in the article's Creative Commons licence and your intended use is not permitted by statutory regulation or exceeds the permitted use, you will need to obtain permission directly from the copyright holder. To view a copy of this licence, visit http://creativecommons.org/licenses/by/4.0/.

© The Author(s) 2024